Materials Chemistry and Physics. Volume 295, 1 February 2023, 127039

https://doi.org/10.1016/j.matchemphys.2022.127039

Fast synthesis of zeolitic imidazolate framework ZIF-94 using NaOH and recycling reagents

Lorena Paseta[1,2], Magdalena Malankowska[1,2,*], Carlos Tellez[1,2], Joaquin Coronas[1,2,*]

[1]Institute of Nanoscience and Materials of Aragon (INMA), University of Zaragoza-CSIC, 50018 Zaragoza, Spain.

[2]Chemical and Environmental Engineering Department, University of Zaragoza, 50018 Zaragoza, Spain.

*Corresponding authors' email: magnal@unizar.es, coronas@unizar.es

Abstract

ZIF-94 is a zeolitic imidazolate framework with the same SOD type topology than ZIF-8 but with an aldehyde group functionalized organic ligand. This turns ZIF-94 less thermally stable than ZIF-8 but with interesting properties of water and carbon dioxide adsorption, making the former a material highly suitable for carbon capture technologies. In this work, an alternative procedure for the synthesis of ZIF-94 was developed based on the use of NaOH as deprotonator. Besides, the crystallization was carried out in a very short time (1-20 min) at room temperature while centrifuging at 10,000 rpm. This made possible the simultaneous crystallization and separation of the product material giving rise, together with the use of the inorganic deprotonator, to a very efficient process with crystallization yields higher than 65 %. For the best conditions tested (crystallization-centrifugation time of 5 min), 66±24 nm in particle size, highly crystalline ZIF-94 with 485 $m^2 \cdot g^{-1}$ of specific surface area was obtained at a crystallization yield of 66.9 %. Similar properties were obtained for ZIF-94 when prepared from recycled reagents (solvent, ligand and Zn salt).

1. INTRODUCTION

Metal organic frameworks (MOFs) are crystalline porous organic-inorganic hybrid materials that attract great attention due to their wide range of potential applications.[1] Due to their composition and structural flexibility MOFs are able to actuate in several different physicochemical fields, showing promising performances in catalysis,[2,3] bioreactors,[4] energy production,[5] solar cells,[6] sensors,[7] diagnosis and controlled drug release,[8] toxicity study[9] as well as gas separation through adsorption and mixed matrix membranes (MMMs),[10] to name

a few. Magnetic MOFs are also gaining popularity. Zeolitic imidazolate framework – graphene oxide nanocomposites, for example, are successfully used for pollutant removal from water,[11] nickel-zinc ferrite or chitosan magnetic nanoparticles can be used for dye degradation.[12] All these applications require excellent and precise control of the synthesis conditions to optimize textural and morphological properties of MOFs. Moreover, MOFs can be patterned to either ensure excellent material positioning or to modify the surface in terms of hydrophobicity and hydrophilicity.[13] The versatility of MOFs relies on their ability to be easily chemically modified for tailoring their functional and textural properties. Zeolite imidazolate frameworks (ZIFs) are a subclass of MOFs comprised of metal cations (Zn^{2+} or Co^{2+}) linked to the nitrogen atoms of deprotonated imidazole molecules creating tetrahedral frameworks into zeolite-like topologies.[14] ZIFs are very attractive due to their extraordinary high thermal and chemical stabilities, flexible structures, easy functionalization and ultramicroporosity.[15] ZIF-94, also called SIM-1 (substituted imidazolate material-1), is constructed from Zn atoms and 4-methyl-5-imidazole-carboxaldehyde links and crystallizes in the SOD topology and has a pore size of ca. 0.26 nm.[16–20] Studies have been carried out for the scaling of this MOF[21] and it can be used in many important industrial and technological applications such as those related to: adsorbent for biomass-derived polyols,[22] biocidal material,[23] catalyst,[24,25] CO_2 adsorbent[19] and filler for MMMs applied to CO_2 capture.[26,27] Currently a typical synthesis of ZIF-94 results in the use of either toxic solvents and high temperature[16] or low temperature but very long crystallization processes of up to 16 h.[21] It should be noted that ZIF-93, with the same metal and ligand as ZIF-94 but with RHO structure, can be synthesized by an alternative green approach involving water as solvent for a relatively short time of 2 h.[28]

In this work, looking for a new and environmentally friendly MOF synthesis procedure,[11] we propose two types of modifications for the synthesis of nano-sized ZIF-94: i) fast, modified traditional method using inorganic deprotonator and ii) ultra-fast procedure under centrifugal acceleration. Both modifications combined or not, give rise to a ZIF-94 with physical and chemical properties comparable to those of the ZIF-94 synthesised by the original method. This procedure allows to decrease the synthesis time dramatically. Besides, to decrease the amount of chemical waste considering environmental reasons,[29,30] the synthesis of ZIF-94 nanocrystals from their recycled mother liquors was studied. Few works have addressed the synthesis of MOFs[27,30–34] from their recycled mother liquors and most of them reported the use of sodium hydroxide, potassium hydroxide or ammonia as deprotonators to favour the nucleation and crystal growth of the material. In this work, sodium hydroxide was used as deprotonator and, as a novelty, the synthesis was carried out by centrifugation as well as the recycling of the mother liquor in the same arrangement. As far as we know, there are not reports dealing with the synthesis of ZIF-94 under these advantageous and green conditions. Besides, as it will be shown along the paper, the combined actions not only save reactants and short the synthesis time but also produce MOF of analogous crystallinity and textural properties than those obtained through the conventional method.

2. EXPERIMENTAL

2.1. Materials

Zinc acetate dihydrate ($Zn(CH_3COO)_2 \cdot 2H_2O$), 98%, and 4-methyl-5-imidazolecarboxaldehyde ($C_5H_6N_2O$), 99%, were purchased from Acros Organics. Tetrahydrofuran (THF), anhydrous, was obtained from Sigma-Aldrich. Methanol, HPLC gradient grade ≥99.9 % was purchased from Honeywell. Sodium hydroxide (NaOH) in the form of pellets were supplied by Carlo Erba reagents. All the chemicals were used as obtained from the manufacturer without any further purification.

2.2. ZIF-94 modified traditional synthesis

ZIF-94 synthesis by Madhav et al.[35] was adapted reducing the original reaction time of 16 h. Briefly, 1.584 g (7.2 mmol) of zinc acetate dihydrate was dissolved in 6 mL of methanol. In a separate vial, 1.584 g (14.4 mmol) of 4-methyl-5-imidazolecarboxaldehyde was dissolved in 15 mL of THF. It has been found that the basic medium of synthesis solution promotes deprotonation of linker and the pH affects the nucleation and crystal growth of ZIFs.[36,37] Therefore, NaOH was added to the original synthesis procedure. NaOH pellets were firstly crushed to obtain powdered NaOH for better mixing in the synthesis suspension. The base was added at a ratio 2:1 (base:Zn molar ratio) to the zinc acetate solution and mixed for approximately 10 min. Next, the entire mixture was added into the pre-stirred ligand dispersion. The final mixture was stirred at room temperature (RT). In order to know how the reaction time influences the characteristics of ZIF-94, the synthesis was carried out at different times: 1, 2, 4 and 8 h. Next, the product was collected in a 50 mL tube and washed once with methanol by centrifugation (Beckman Coulter Allegra x-30) at 10,000 rpm during 10 min at RT. Finally, ZIF-94 nanocrystals were activated with 100 mL of EtOH by refluxing during 6 h, collected by centrifugation at 10,000 rpm during 10 min and dried overnight at RT.

2.3. ZIF-94 synthesis by centrifugation

Firstly, two dissolutions were prepared. On one hand, 528 mg (2.4 mmol) of zinc acetate dehydrate and 193 mg (4.8 mmol) of NaOH were dissolved in 2 mL of MeOH. On the other hand, 528 mg (4.8 mmol) of 4-methyl-5-imidazolecarboxaldehyde was dissolved in 5 mL of THF. Subsequently, both solutions were mixed in a 50 mL centrifuge flask. The resultant solution was immediately centrifuged at 10,000 rpm and RT for different times: 1, 3, 5, 7, 10 and 20 min. Finally, the ZIF-94 nanocrystals obtained were activated following the same procedure as in the case of the traditional ZIF-94 synthesis (see Figure 1 for detailed scheme of the synthesis and Table S1).

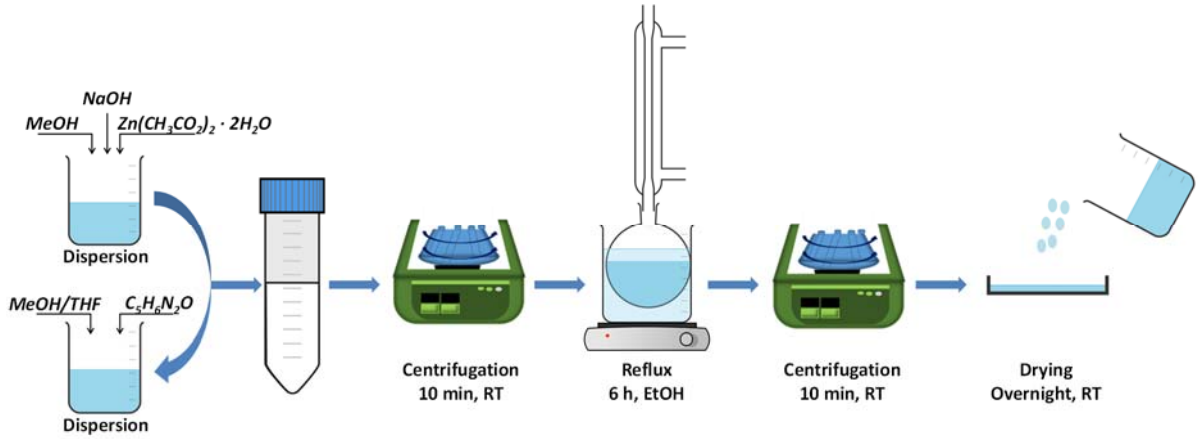

Figure 1: Schematic representation of the ZIF-94 synthesis with centrifuge

2.4. ZIF-94 synthesis by centrifugation from recycled mother liquor

After the synthesis of ZIF-94 by centrifugation, the mother liquors obtained were recovered and reused for the subsequent synthesis of ZIF-94. The main aim of this procedure was to save reagents (solvent, ligand and Zn salt) and simultaneously synthesize ZIF-94 from these mother liquors keeping its morphology, textural properties and particle size as similar to the original ZIF-94 as possible. To do that, once the synthesized nanocrystals were recovered, thermogravimetry (see below) was used to calculate the percentage of pure ZIF-94 synthesized (i.e. excluding trapped solvent and ligand). Once this percentage was known, the amount of unreacted reagents was calculated by mass balance taking into account the stoichiometry of the reaction (Eq. 1) ($C_5H_6N_2O$ being 4-methyl-5-imidazolecarboxaldehyde), and the required amount of those reagents were added together with the volume of the lost solvent.

$$Zn(CH_3CO_2)_2 \cdot 2H_2O + 2C_5H_6N_2O \rightarrow Zn(C_5H_5N_2O)_2 + 2H^+ + 2CH_3CO_2^- + 2H_2O \qquad \text{(Eq. 1)}$$

Besides, as can be seen in Eq. 1, acetic acid is produced as a byproduct of the reaction, so the pH of the medium would decrease during the synthesis, unless NaOH is added as a base[35] to reestablish the pH of the mother liquors as well as to favor the deprotonation of the organic ligand.

2.5. Characterization of samples

Powder X-ray diffraction data of nano-sized ZIF-94 were collected using Panalytical Empyrean equipment with CuKα radiation (λ = 0.154 nm), over the range of 5º - 40º at a scan rate of 0.03º s^{-1}. Thermogravimetric analyses (TGA) were carried out using a Mettler Toledo TGA/STDA 851e. A small amount of the sample (approx. 5 mg) placed in a 70 µL alumina pan was heated under airflow (40 mL(STP) min^{-1}) from 35 to 700 °C at a heating rate of 10 °C min^{-1}. Normalized weight versus temperature curve was plotted. N_2 adsorption-desorption isotherms were obtained using a Micromeritics TriStar 3000 at 77 K. Before these measurements, ZIF-94 samples were degassed for 8 h under vacuum at 200 °C using a heating

rate of 10 °C min^{-1}. The surface area was calculated using the Brunauer-Emmett-Teller (BET) method. The morphology of ZIF-94 nanoparticles was examined by scanning electron microscopy (SEM) with backscattered electron mode using an Inspect F50 model scanning microscope (FEI), operated at 10 kV. The particle size was calculated measuring minimum 80 particles using ImageJ 1.49b software. In addition, the samples were analyzed through transmission electron microscopy (TEM). The sample suspension in methanol was placed onto a carbon-coated copper 300 mesh TEM grid and observed with FEI Tecnai T20 operated at 200 kV.

The Scherrer equation was used to calculate the crystallite size from XRD patterns:

$$L = \frac{K \cdot \lambda}{\beta \cdot cos\theta} \quad \text{(Eq. 2)}$$

where L is the crystallite size (nm), K is a constant (0.96), λ is the X-ray wavelength (nm), β is the full width at half maximum (FWHM) intensity (radians) and θ is the diffraction angle (radians).

Furthermore, considering a calculation base of 100 g of synthesis mixture, the yield of the reaction was defined as the ratio of the amount of solid ZIF-94 obtained ("Exp. ZIF-94") to the maximum possible amount of ZIF-94 that can be produced if all limiting reactants (Zn^{2+} or ligand, both are in stoichiometric quantity) are consumed ("Theor. ZIF-94") according to the following equation:

$$Yield\ (\%) = \frac{Exp.\ ZIF{-}94}{Theor.\ ZIF{-}94} \cdot 100 \quad \text{(Eq. 3)}$$

3. RESULTS AND DISCUSSION

As it was mentioned in the experimental section, two types of syntheses were conducted in this study: i) fast modified traditional method using an inorganic deprotonator and ii) ultra-fast synthesis by centrifugation. Figure 2 shows a scheme of all the experiments conducted in this work. The synthesis approaches were divided into two methods: Method A, corresponding to the use of inorganic deprotonator NaOH with the modified traditional method, and Method B, corresponding to the use of a centrifuge. The synthesis time was studied and such examination resulted in the formation of different products: A.1-A.5 for Method A and B.1-B.6 for Method B as well as in the case of the recycled mother liquors: product B.5 (recycled).

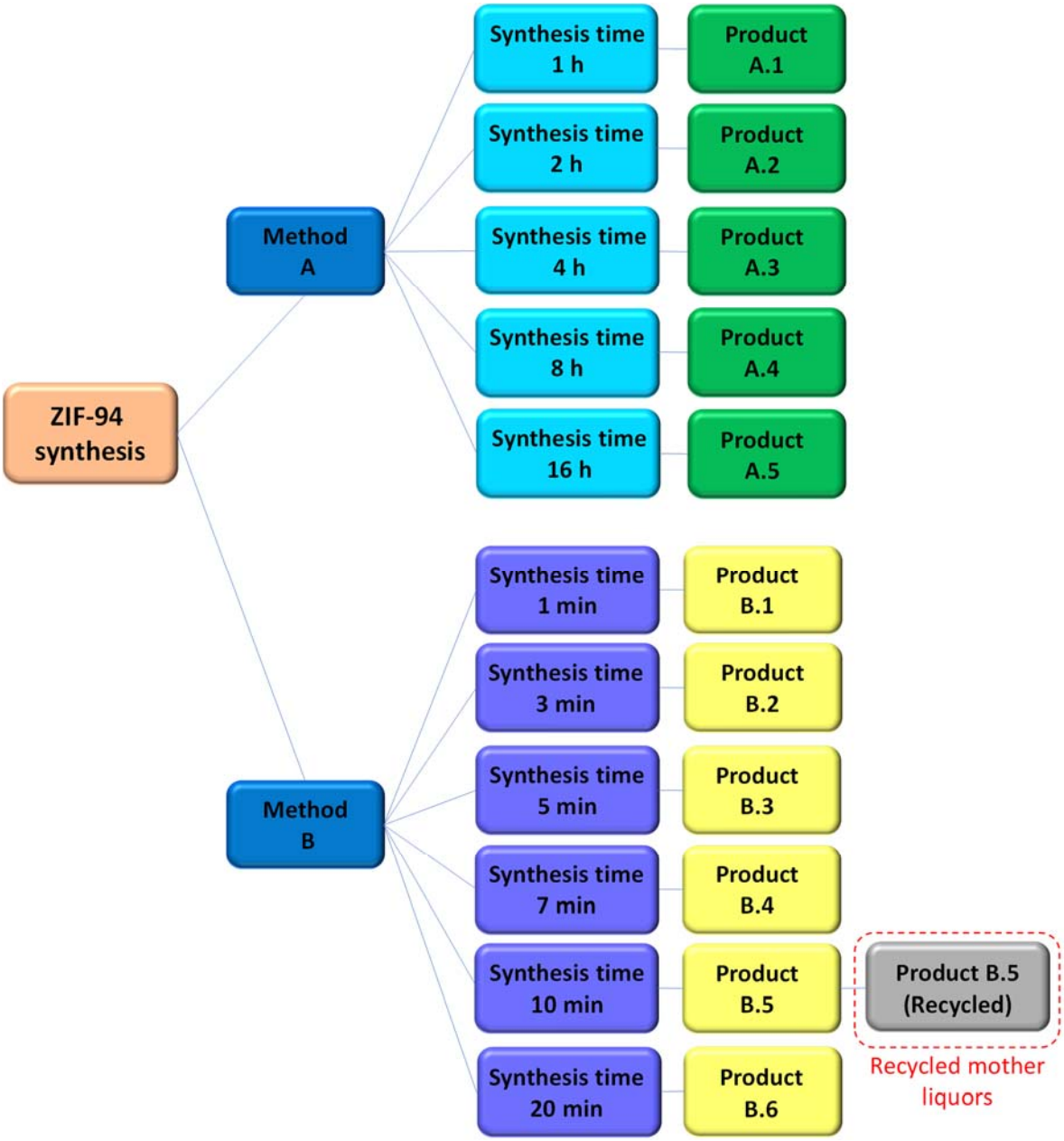

Figure 2: Schematic representation of the syntheses conducted in this work. Method A corresponds to the synthesis based on the use of an inorganic deprotonator and Method B based on the use of a centrifuge and an inorganic deprotonator.

3.1. Modification A

3.1.1. ZIF-94 characterization

Previous studies have already shown that the presence of NaOH deprotonates the imidazole ligand and accelerates nucleation and crystallization, thereby reducing the particle size in respect to traditional methods without deprotonators. The ratio 2:1 (NaOH:Zn) resulted in optimized values of surface area and for this reason this ratio has been chosen in method A.[35] The crystalline structure of the ZIF-94 synthesized at different times was determined by X-ray diffraction. Figure 3A depicts the XRD patterns of all the products obtained by method A that are consistent with the simulated pattern.[38] This confirms high crystallinity of the samples and that all the materials share the SOD type structure

corresponding to ZIF-94.[38] The thermal stability was determined by TGA (Figure 3B), where two weight losses can be appreciated. One from 35 °C to 180 °C, corresponding to the removal of the solvents (MeOH and THF) used in the synthesis, and another one from 250 °C to about 550 °C, due to the MOF degradation until obtaining ZnO as final residue since the TGA was carried out in air. Besides, the TGA curves do not suggest the presence of traces of unreacted linker inside the pores indicating that all products were well activated. Note that the TGA curves along the paper show differences below ca. 200 °C due the hydrophilic character of ZIF-94 which provokes retention of water and polar solvents. In any event, the TGA curves shown here and along the paper are similar to those of other ZIF-94 samples previously published,[27,35] in line with the high crystallinity of the MOF achieved.

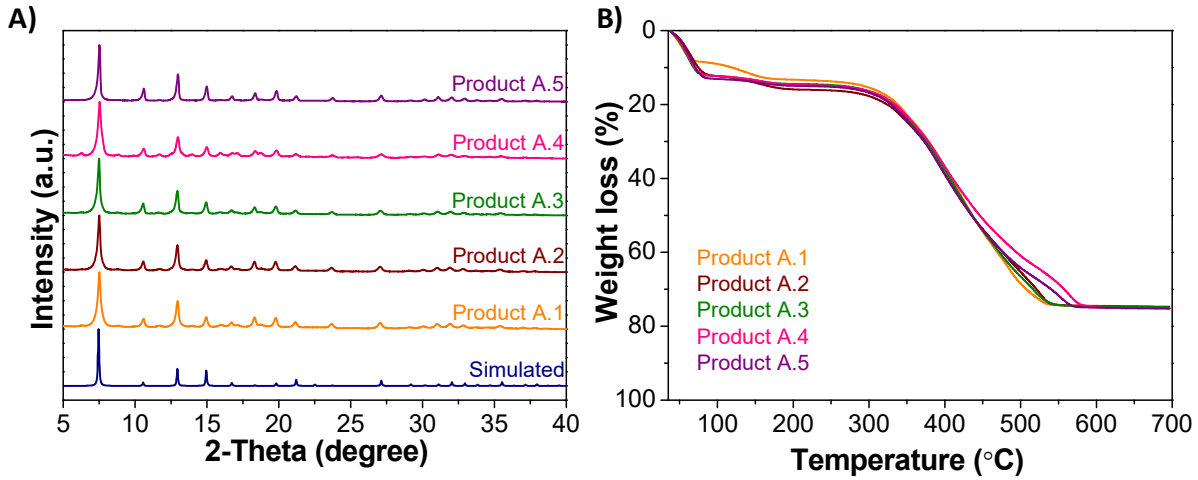

Figure 3: Products A.1, A.2, A.3, A.4 and A.5: A) XRD patterns, and B) TGA curves.

SEM images (see Figure 4) show that the reaction time did not affect the apparent morphology of the nanoparticles obtained and all the obtained products exhibit the morphology described in the literature, i.e. the crystals exhibit a rombododecahedral shape.[35] Besides, these SEM images were used to calculate average particle sizes. As can be seen in Table 1The yield of all carried out syntheses was calculated applying Eq. 3. The higher the reaction time, the higher the yield. In any event, both SEM observations and Scherrer calculations are consistent with a growth of the particle size of ZIF-94 with the crystallization time. Moreover, the higher the consumption of the reactants the higher the crystallization yields (74.2-83.8 % for products A.1-A.5, see Table 1). Besides, the BET specific surface areas are between 419 and 507 m2·g-1, in the range of the values reported in the literature (415-571 m2·g-1). [18,21,27,35,39] These values, and the similar ones shown along the paper, together with the high crystallinity of the ZIF-94 samples, suggest that the adsorption performance of materials achieved in this work for any typical adsorbate by applying the new synthesis methodology would be comparable to that corresponding to ZIF-94 prepared by conventional synthetic routes.

Table , the particle size increases with increasing synthesis time, being 49, 47, 51, 55 and 58 nm from product A.1 to product A.5, respectively. The calculation of the particle size applying Scherrer equation (Eq. 2) revealed that the dimensions should be in the range of 36-

49 nm, which is slightly lower than the values obtained by SEM. This discrepancy suggests the formation of ZIF-94 agglomerates that would not be suitable for characterizations such as DLS. In fact, this is in agreement with the SEM characterization where, beyond the average values given above, with relatively large errors (see Table 1), some large particles of about 100-200 nm are visible. The calculated values are in agreement with TEM images showing nanoparticles in the same size range (Figure S1),[27] and where it is also possible to visualize little bubbles due to the burning of the samples during the observation. These nanoparticles would constitute the SEM agglomerates (clearly not single crystals, in agreement with previous studies based on Le Bail calculations)[26] observed without discarding the presence of ZIF-94 single crystals of ca. 100-200 nm.

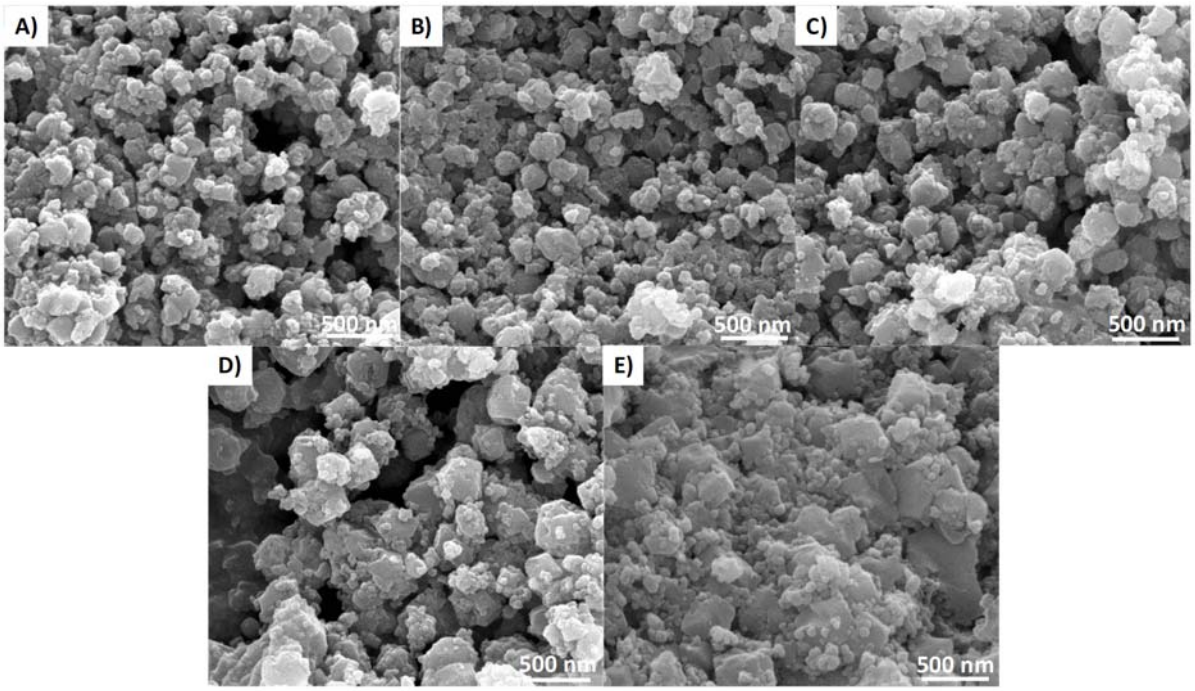

Figure 4: SEM images of products A.1-A.5 (A-E).

The yield of all carried out syntheses was calculated applying Eq. 3. The higher the reaction time, the higher the yield. In any event, both SEM observations and Scherrer calculations are consistent with a growth of the particle size of ZIF-94 with the crystallization time. Moreover, the higher the consumption of the reactants the higher the crystallization yields (74.2-83.8 % for products A.1-A.5, see Table 1). Besides, the BET specific surface areas are between 419 and 507 $m^2 \cdot g^{-1}$, in the range of the values reported in the literature (415-571 $m^2 \cdot g^{-1}$). [18,21,27,35,39] These values, and the similar ones shown along the paper, together with the high crystallinity of the ZIF-94 samples, suggest that the adsorption performance of materials achieved in this work for any typical adsorbate by applying the new synthesis methodology would be comparable to that corresponding to ZIF-94 prepared by conventional synthetic routes.

Table 1: Mean particle size, crystallite size, BET specific surface area (SSA) and yield for the samples synthesized by method A.

Sample	Mean particle size (SEM) (nm)	Crystallite size (Scherrer equation) (nm)	BET SSA ($m^2 \cdot g^{-1}$)	Yield (%)
A.1	49±17	36	419	74.2
A.2	47±14	39	428	74.1
A.3	51±17	41	494	76.3
A.4	55±15	33	507	77.4
A.5	58±26	49	478	83.8

3.2. Modification B

3.2.1. ZIF-94 characterization

In order to investigate if it was possible to further decrease the synthesis time, MOF crystallization was carried out by a centrifugation method. Sánchez-Laínez et al.[40] performed the synthesis of nano ZIF-11 by centrifugation and achieved a reduction of the synthesis time from 3 h in the original synthesis to only 1 min. However, the authors were not able to obtain an XRD-crystalline phase but nanoparticles of an amorphous phase with the same chemical composition of ZIF-11 and analogous but reduced CO_2 adsorption properties were obtained. In our case, we studied 6 different synthesis times: 1, 3, 5, 7, 10 and 20 min (see samples B.1 to B.6 in Figure 2) and we were able to obtain XRD crystalline ZIF-94. The decrease in synthesis time is related to the crystallization rate. A possible explanation is that the centrifugal force helps to reduce the stagnant liquid film surrounding the growing crystal, thus avoiding abrupt concentration profiles, which increases the mass transfer rate of the reactants and therefore the rate of crystallization.

Figure 5A shows the XRD patterns of the products obtained for each synthesis time of this study. In all cases, the results are congruent with the simulated XRD pattern corresponding to ZIF-94. Even when the synthesis was carried out during 1 min, a crystalline material was obtained. Figure 5B depicts the thermal stability of the obtained products as determined by TGA. It could be appreciated that all the products have almost the same thermal stability (around 250 °C) with the same two weight losses as the materials prepared with the modified traditional method A.

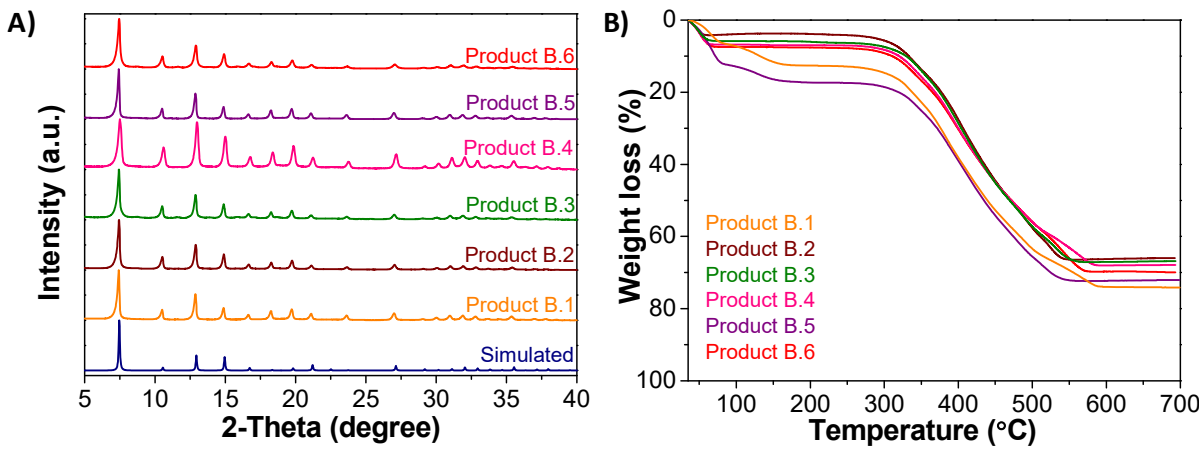

Figure 5: Products B.1, B.2, B.3, B.4, B.5 and B.6: A) XRD patterns, and B) TGA curves.

SEM images of the obtained products are shown in Figure 6. For all the different synthesis times explored in this study, the particle morphology is similar to that achieved by the traditional synthesis shown above with crystals with the typical rombododecahedral shape, sometimes not very clearly discerned due to the presence of MOF agglomerates. Table 2 shows the mean particle size of all the products synthesized. As can be seen, the longer the synthesis time, the larger the particle size. Although, for a synthesis time of 7 min, the particle size was stabilized at around 69 nm. In all cases, the particle size is slightly larger than that obtained when the synthesis was carried out by method A, except in the case of synthesis time of 16 h. In this case, the particle size is in the range of the one obtained by method B. Applying the Scherrer equation (Eq. 2), the particle size of the products obtained by method B should be in the range of 34-50 nm, which again indicates the formation of ZIF-94 agglomerates, in agreement with the SEM characterization showing average particle sizes in the 60-72 nm range. Once more, TEM images (see Figure S2) show similar findings to those observed for the regular synthesis, i.e. crystallite sizes closer to the values calculated by Scherrer equation, confirming the already quoted agglomeration.

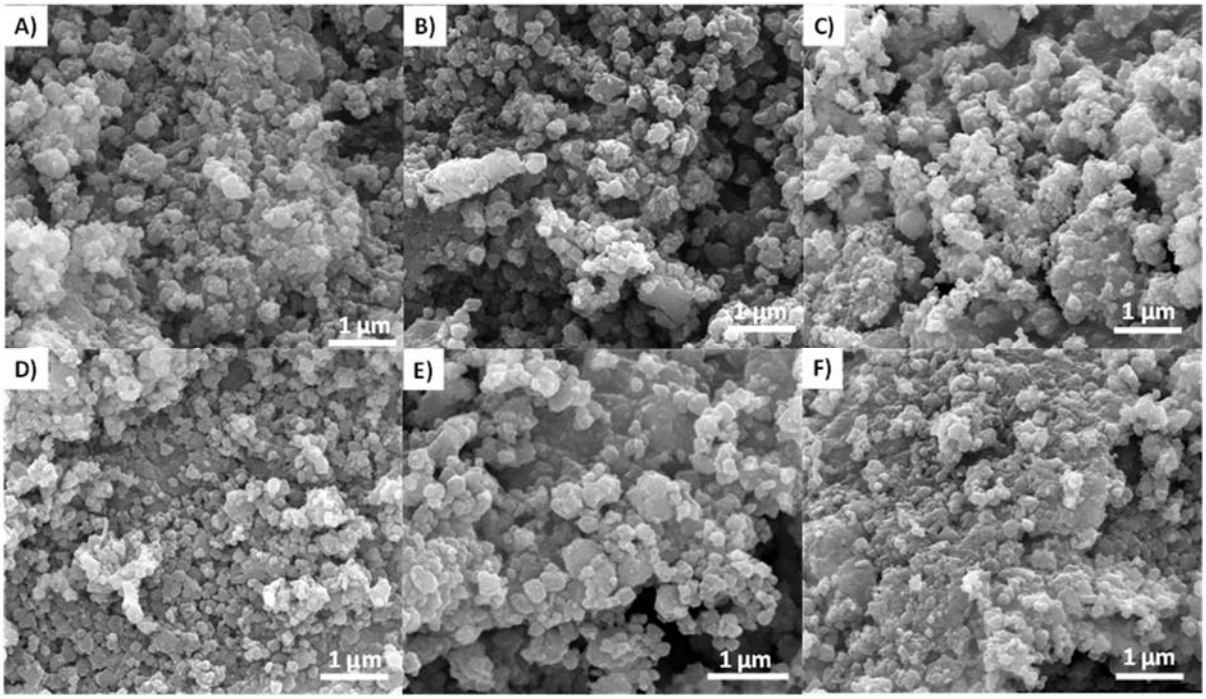

Figure 6: SEM images of products B.1-B.6 (A-F).

In parallel with the analysis done with method A samples, the BET specific surface areas are again within the range reported in literature, between 412 and 485 $m^2 \cdot g^{-1}$ (Table 2). Similarly, the yields, between 62.9% and 66.9%, are close to the one obtained by method A for synthesis times of 1 h (74.2%) and 2 h (74.1%), indicating that method B was faster than method A as it was possible to obtain a very similar performance in terms of crystallization yield, crystallinity, thermal stability and textural properties but with a shorter synthesis time. Finally, the centrifugation during the crystallization of MOF separates the obtained crystals (going to the bottom of the centrifuge tube) from the mother liquors what tends to stop the growing of the first MOF particles, justifying the lower yield obtained with method B. In other words, the synthesis durations in the range of a few minutes are quite accurate since the simultaneous synthesis and separation by centrifugation avoids subsequent contact of the solid product with the nutrient solutions. Finally, mean particle sizes are in the range of a few tens of nanometers as those obtained in previous works, in some cases dealing with the preparation of MMMs where the nanometer size is of paramount importance.[26,27,35]

Table 2: Mean particle size, crystallite size, BET SSA and yield for the samples synthesized by method B. Run "B.5 (recycled)" used the crystallization mother liquors.

Sample	Mean particle size (SEM) (nm)	Crystallite size (Scherrer equation) (nm)	BET SSA ($m^2 \cdot g^{-1}$)	Yield (%)
B.1	60±16	39	440	62.9
B.2	63±19	45	483	65.7
B.3	66±24	44	485	66.9

B.4	69±20	34	417	66.7
B.5	72±25	50	412	66.0
B.5 (recycled)	61±20	39	466	46.8
B.6	69±22	34	468	65.1

3.2.2. Characterization of the ZIF-94 synthesized from recycled mother liquors

Taking into account that the yield of the crystallization reaction is not 100% (see Table), it is clear that unreacted reagents are present in the mother liquors. Similarly to our previous work, where we synthesized ZIF-94 by recycling mother liquors,[27] we have tried to repeat the procedure, but this time, using method B developed in the present work, which applies a centrifuge to carry out the synthesis. This would confirm that the recycling methodology would also apply for a ZIF-94 synthesis procedure requiring just a few minutes of reaction, simultaneously carrying out the crystallization and the separation of the crystal products from the corresponding mother liquors. Even if 2-10 min synthesis times produced similar results with syntheses yields in the 65.7-66.9% range, the synthesis time selected for this study was 10 min, i.e. corresponding to product B.5 in method B with suitable textural and morphological features. This time resulted simply more comfortable from the operational point of view and was still far lower from the conventional synthesis time. This run is denoted as “B.5 (recycled)” in Table 2 and Figure 2.

Figure 7A shows the XRD pattern of products B.5 and B.5 (recycled), corresponding to the solid obtained by recycling the mother liquor from B.5 synthesis. The XRD pattern of the recycled product B.5 matches well with both the XRD of the synthesis with fresh reagents and the one simulated from crystallographic data. In Figure 7B the thermogravimetric analysis of the product B.5 (recycled) can be seen. As in the case of product B.5 and the other products obtained in this work by methods A and B without recycling (Figure 3B and Figure 5B), the weight loss curve shows the same two main steps from 35 °C to 180 °C, corresponding to the solvents present in the mother liquor, and from 250 °C to ca. 550 °C due to the MOF degradation. Therefore, it can be concluded that the recycled product preserves the thermal resistance of ZIF-94 from the original synthesis.

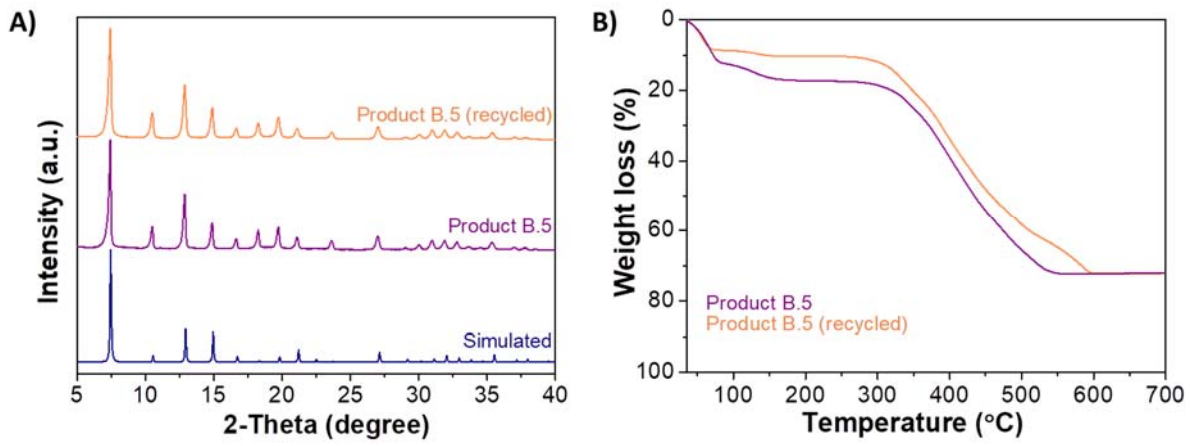

Figure 7: Products B.5 and B.5 (recycled): A) XRD patterns, and B) TGA curves.

Figure S3 shows an SEM image of product B.5 (recycled). The nano-sized ZIF-94 obtained from the reused mother liquor exhibits the expected morphology obtained with methods A and B. Moreover, the mean particle size obtained was equal to 61 nm (see Table 2). Even though the particle size of product B.5 (recycled) is slightly smaller than that of the solid obtained by the regular procedure, it is within the range corresponding to the samples obtained by method B at different synthesis times. Besides, as it happened in previous products, the solid obtained seems to be agglomerated since the crystallite size according to the Scherrer equation (Eq. 2) should be 39 nm.

The BET specific surface area of product B.5 (recycled) equal to 466 $m^2 \cdot g^{-1}$ is in good agreement with the above presented values, being even slightly higher than the ones obtained in the regular synthesis without recycling. See also similar N_2 adsorption isotherms (type I with small hysteresis) for the for the two B.5 products shown in Figure S4. Moreover, the synthesis yield is lower than the one obtained in the ZIF-94 synthesis without recycling, being 46.8 % for the first one and 66.0% for the last one. This decrease in the crystallization yield of the MOF obtained from recycled mother liquors has been reported in the literature, not only for ZIF-94,[27] but also for other MOFs like ZIF-8,[32,34] ZIF-67,[32] ZIF-7[32] or ZIF-L.[32] As Eq. 1 shows, acetic acid is formed during the synthesis, which is in turn neutralized with NaOH giving rise to sodium acetate. When reusing the mother liquor, this salt is accumulated in the reaction medium increasing the ionic strength of the solution. This may hinder the interaction between Zn and ligand species in the conditions tested here. In any event, the global yield considering both consecutive syntheses as a global process was 67.9%, meaning that the absolute amount of ZIF-94 was higher per fresh reagents unit. In fact, the grams of ZIF-94 per gram of hydrated zinc salt were 0.85, 0.85 and 0.88 for the B.5 synthesis, B.5 (recycle) and considering both consecutive syntheses (see Table S2). On the other hand, the grams of ZIF-94 per gram of solvent for the same three situations were 0.075, 0.075 and 0.096, respectively. These calculations highlight the advantage of the recycling approach followed in this work to synthesize MOF ZIF-94.

4. Conclusion

In this work, two modifications for the synthesis of ZIF-94 were carried out. The first, used an inorganic deprotonator added to the traditional synthesis together with a significant decrease of the synthesis time (method A) and the second one was carried out by centrifugation (method B), i.e. simultaneously achieving the crystallization and the separation of crystals from mother liquor.

Regardless of the reaction time, method A produced ZIF-94 with similar properties in terms of crystallinity, thermal stability, morphology, particle size and BET specific surface area to the ZIF-94 synthesized by a traditional method (i.e. with toxic solvents or very long reaction time). Considering the yield, the longer the reaction time, the higher the yield, within the 74.2-83.8% range. When applying the centrifugation procedure (method B), the reaction times were reduced from several hours to 1-20 min. As in the case of method A, for all the reaction times in this study, ZIF-94 was obtained. Even for 1 min synthesis the XRD showed a crystalline product with all the features corresponding to the SOD type structure. The products synthesized by method B exhibited similar morphology, thermal stability and BET specific surface area to those obtained by method A, whereas the particle size was slightly larger. The yield values are close to those achieved by method A. This allowed to conclude that method B was clearly faster than method A resulting in the production of similar products.

Finally, the synthesis of ZIF-94 from a recycled mother liquor gave rise to a solid with crystallinity, thermal stability and textural properties relatively similar to those of the parent product; although the yield was lower, what could be attributed to the accumulated sodium acetate altering the ionic strength of the reaction medium and thus the reaction between the ZIF precursors in the studied conditions. In any case, the synthesis of the recycled mother liquor would save reactants, which would lead to a more sustainable synthesis with a higher production of MOF per unit reagents. In addition, the synthesis with centrifugation, which, as mentioned includes separation, is a process that can be easily scaled up in a continuous process for the production of MOFs which can include the recirculation of unreacted reagents. This more sustainable and easier upscaling will facilitate the economical industrial application of ZIF-94 and other related materials prepared under similar conditions.

Acknowledgements:

Grant PID2019-104009RB-I00 funded by MCIN/AEI/10.13039/501100011033 from the Spanish Agencia Estatal de Investigación (AEI) is gratefully acknowledged. The authors would like to acknowledge the use of the Servicio General de Apoyo a la Investigación-SAI and the use of instrumentation as well as the technical advice provided by the National Facility ELECMI ICTS, node "Laboratorio de Microscopias Avanzadas" at the University of Zaragoza.

References:

1 D. Bazer-Bachi, L. Assié, V. Lecocq, B. Harbuzaru and V. Falk, *Powder Technol.*, 2014, **255**, 52–59.

2 J. Gascon, A. Corma, F. Kapteijn and F. X. Llabrés i Xamena, *ACS Catal.*, 2014, **4**, 361–378.

3 H. N. Abdelhamid and A. P. Mathew, *Coord. Chem. Rev.*, 2022, **451**, 214263.

4 C. M. Doherty, G. Grenci, R. Riccò, J. I. Mardel, J. Reboul, S. Furukawa, S. Kitagawa, A. J. Hill and P. Falcaro, *Adv. Mater.*, 2013, **25**, 4701–4705.

5 S. K. Henninger, F. Jeremias, H. Kummer and C. Janiak, *Eur. J. Inorg. Chem.*, 2012, **2012**, 2625–2634.

6 C.-C. Chueh, C.-I. Chen, Y.-A. Su, H. Konnerth, Y.-J. Gu, C.-W. Kung and K. C.-W. Wu, *J. Mater. Chem. A*, 2019, **7**, 17079–17095.

7 L. E. Kreno, K. Leong, O. K. Farha, M. Allendorf, R. P. Van Duyne and J. T. Hupp, *Chem. Rev.*, 2012, **112**, 1105–1125.

8 P. Horcajada, R. Gref, T. Baati, P. K. Allan, G. Maurin, P. Couvreur, G. Férey, R. E. Morris and C. Serre, *Chem. Rev.*, 2012, **112**, 1232–1268.

9 F. E.-Z. A. Abd El-Aziz, N. E. Ebrahem and H. N. Abdelhamid, *Sci. Rep.*, 2022, **12**, 14240.

10 R. Lin, B. Villacorta Hernandez, L. Ge and Z. Zhu, *J. Mater. Chem. A*, 2018, **6**, 293–312.

11 N. M. Mahmoodi, M. Oveisi, M. Bakhtiari, B. Hayati, A. A. Shekarchi, A. Bagheri and S. Rahimi, *J. Mol. Liq.*, 2019, **282**, 115–130.

12 N. M. Mahmoodi, M. Bashiri and S. J. Moeen, *Mater. Res. Bull.*, 2012, **47**, 4403–4408.

13 C. L. Ruiz-Zambrana, M. Malankowska and J. Coronas, *Dalt. Trans.*, 2020, **49**, 15139–15148.

14 Y.-R. Lee, J. Kim and W.-S. Ahn, *Korean J. Chem. Eng.*, 2013, **30**, 1667–1680.

15 A. M. Coclite, R. M. Howden, D. C. Borrelli, C. D. Petruczok, R. Yang, J. L. Yagüe, A. Ugur, N. Chen, S. Lee, W. J. Jo, A. Liu, X. Wang and K. K. Gleason, *Adv. Mater.*, 2013, **25**, 5392–5423.

16 S. Aguado, J. Canivet and D. Farrusseng, *Chem. Commun.*, 2010, **46**, 7999–8001.

17 H. Amrouche, S. Aguado, J. Pérez-Pellitero, C. Chizallet, F. Siperstein, D. Farrusseng, N. Bats and C. Nieto-Draghi, *J. Phys. Chem. C*, 2011, **115**, 16425–16432.

18 A. M. Marti, M. Van and K. J. Balkus, *J. Porous Mater.*, 2014, **21**, 889–902.

19 W. Morris, N. He, K. G. Ray, P. Klonowski, H. Furukawa, I. N. Daniels, Y. A. Houndonougbo, M. Asta, O. M. Yaghi and B. B. Laird, *J. Phys. Chem. C*, 2012, **116**, 24084–24090.

20 A. Sabetghadam, X. Liu, M. Benzaqui, E. Gkaniatsou, A. Orsi, M. M. Lozinska, C. Sicard, T. Johnson, N. Steunou, P. A. Wright, C. Serre, J. Gascon and F. Kapteijn, *Chem. – A Eur. J.*, 2018, **24**, 7949–7956.

21 T. Johnson, M. M. Łozińska, A. F. Orsi, P. A. Wright, S. Hindocha and S. Poulston, *Green*

Chem., 2019, **21**, 5665–5670.

22 H. Jin, Y. Li and W. Yang, *Ind. Eng. Chem. Res.*, 2018, **57**, 11963–11969.

23 K. Martín-Betancor, S. Aguado, I. Rodea-Palomares, M. Tamayo-Belda, F. Leganés, R. Rosal and F. Fernández-Piñas, *Sci. Total Environ.*, 2017, **595**, 547–555.

24 S. Aguado, J. Canivet and D. Farrusseng, *J. Mater. Chem.*, 2011, **21**, 7582–7588.

25 H. N. Abdelhamid, *Appl. Organomet. Chem.*, 2022, **36**, e6753.

26 M. Etxeberria-Benavides, O. David, T. Johnson, M. M. Łozińska, A. Orsi, P. A. Wright, S. Mastel, R. Hillenbrand, F. Kapteijn and J. Gascon, *J. Memb. Sci.*, 2018, **550**, 198–207.

27 M. R. Hasan, L. Paseta, M. Malankowska, C. Téllez and J. Coronas, *Adv. Sustain. Syst.*, 2021, **n/a**, 2100317.

28 E. V Ramos-Fernandez, A. Grau-Atienza, D. Farrusseng and S. Aguado, *J. Mater. Chem. A*, 2018, **6**, 5598–5602.

29 N. Tannert, S. Gökpinar, E. Hastürk, S. Nießing and C. Janiak, *Dalt. Trans.*, 2018, **47**, 9850–9860.

30 S. Gökpinar, T. Diment and C. Janiak, *Dalt. Trans.*, 2017, **46**, 9895–9900.

31 N. Keser Demir, B. Topuz, L. Yilmaz and H. Kalipcilar, *Microporous Mesoporous Mater.*, 2014, **198**, 291–300.

32 F. Şahin, B. Topuz and H. Kalıpçılar, *Microporous Mesoporous Mater.*, 2018, **261**, 259–267.

33 N. Jamil, N. H. Alias, M. Z. Shahruddin and N. H. Othman, *Key Eng. Mater.*, 2019, **797**, 48–54.

34 M. García-Palacín, J. I. Martínez, L. Paseta, A. Deacon, T. Johnson, M. Malankowska, C. Téllez and J. Coronas, *ACS Sustain. Chem. Eng.*, 2020, **8**, 2973–2980.

35 D. Madhav, M. Malankowska and J. Coronas, *New J. Chem.*, 2020, **44**, 20449–20457.

36 M. C. McCarthy, V. Varela-Guerrero, G. V Barnett and H.-K. Jeong, *Langmuir*, 2010, **26**, 14636–14641.

37 S. R. Venna, J. B. Jasinski and M. A. Carreon, *J. Am. Chem. Soc.*, 2010, **132**, 18030–18033.

38 M. Baias, A. Lesage, S. Aguado, J. Canivet, V. Moizan-Basle, N. Audebrand, D. Farrusseng and L. Emsley, *Angew. Chemie Int. Ed.*, 2015, **54**, 5971–5976.

39 W. Morris, B. Leung, H. Furukawa, O. K. Yaghi, N. He, H. Hayashi, Y. Houndonougbo, M. Asta, B. B. Laird and O. M. Yaghi, *J. Am. Chem. Soc.*, 2010, **132**, 11006–11008.

40 J. Sánchez-Laínez, B. Zornoza, Á. Mayoral, Á. Berenguer-Murcia, D. Cazorla-Amorós, C. Téllez, J. J. Coronas, J. Sanchez-Lainez, B. Zornoza, A. Mayoral, A. Berenguer-Murcia, D. Cazorla-Amoros, C. Tellez and J. J. Coronas, *J. Mater. Chem. A*, 2015, **3**, 6549–6556.